Applied Catalysis B: Environmental 294 (2021) 120255

Contents lists available at ScienceDirect

Applied Catalysis B: Environmental

journal homepage: www.elsevier.com/locate/apcatb

Inside the reaction mechanism of direct CO_2 conversion to DME over zeolite-based hybrid catalysts

G. Bonura [a,*], S. Todaro [a,b], L. Frusteri [a], I. Majchrzak-Kucęba [c], D. Wawrzyńczak [c], Z. Pászti [d], E. Tálas [d], A. Tompos [d], L. Ferenc [d], H. Solt [d], C. Cannilla [a], F. Frusteri [a]

[a] CNR-ITAE, Istituto di Tecnologie Avanzate per l'Energia "Nicola Giordano", Via S. Lucia sopra Contesse 5, 98126, Messina, Italy
[b] Università della Calabria, Dip. Ing. Ambiente Territorio e Ing. Chimica, Via P. Bucci, 87036, Rende, Italy
[c] Częstochowa University of Technology, Department of Advanced Energy Technologies, Dąbrowskiego 73 St., 42-201, Częstochowa, Poland
[d] Institute of Materials and Environmental Chemistry, Research Centre for Natural Sciences, Magyar tudósok körútja 2, H-1117, Budapest, Hungary

ARTICLE INFO

Keywords:
Hybrid catalysts
CO_2 conversion
DME production
Reaction mechanism
Operando spectroscopy

ABSTRACT

This paper aims at shedding more light on the reaction mechanism behind the direct hydrogenation of CO_2 streams into DME in presence of hybrid catalysts. Starting from the physico-chemical properties of an optimized CuO-ZnO-ZrO_2/HZSM-5 catalytic system, whose synergy among active sites of different nature (i.e., metal/oxide and acid/base) was recently proposed as the key to overcome the typical limitations showed by random mixing of two preformed catalysts, new evidences are herewith reported about catalytic performance, conditions for activation of reactants, limiting steps and product formation. Likewise to other proposed mechanisms at the state of the art, the catalyst efficiency is resulted to be dependent on several catalyst features, related not only to the metal-oxide phase responsible for CO_2 activation/hydrogenation, but also to specific characteristics of the zeolite (i.e., porosity, specific surface area, population, location and strength of acid sites, interaction with active metals, …), influencing the activity-selectivity pattern. The production of DME is conditioned by the rate of methanol formation in proximity of the metal-oxide interface, followed by a rapid transferring of methanol towards the neighboring acid sites of the zeolite. Operando spectroscopic investigations performed under simulated reaction conditions (30 bar, 200−260 °C) have shown that the intermediates formation strongly depends upon a concurrence of texture, structure and surface aspects; however, depending on the reaction conditions, methanol formation normally passes through the formation of formate species. From a technological point of view, a reaction pressure of 30 bar appears as the ideal compromise between CO_2 conversion and limitation of operative costs, while, due to thermodynamic restrictions, a reaction temperature not higher than 200 °C is necessary to attain DME selectivity close to 90 %.

1. Introduction

The sustainable production of alternative clean energy vectors represents a topic of great global interest both for economic and environmental concerns. In this context, in recent years particular attention has been paid to the possibility of using DME as an alternative fuel to be used mainly in diesel engines [1–5]. DME is considered an environmentally friendly fuel because it is not toxic, it is not a greenhouse gas and if used in diesel it produces less particulate matter. In addition, DME is a low pressure liquefiable gas and can be easily distributed using the methods already used for LPG [6,7]. DME is currently produced industrially in two steps: 1) synthesis of methanol from synthesis gas; 2) dehydration of methanol on acid systems [8–18]. As it is known, synthesis gases are produced by reforming processes of fossil fuels and therefore the problem of emission of CO_2 in the atmosphere remains [19–21].

Some years ago, a futuristic perspective on the use of CO_2 as a feedstock for methanol production has been proposed [22–25]. This idea focuses on three main aspects: 1) CO_2 capture; 2) the production of hydrogen from renewable sources; 3) the combination of CO_2 and H_2 to produce CH_3OH. In this way, using methanol as the basis for the production of fuels, one could hypothesize a zero-emission of CO_2 cycle. The production of CH_3OH from syngas is a well-known industrial process and CuO-ZnO-Al_2O_3 is the catalyst formulation conventionally used. This catalyst appears to be active also in the synthesis of CH_3OH by using

* Corresponding author.
E-mail address: giuseppe.bonura@itae.cnr.it (G. Bonura).

https://doi.org/10.1016/j.apcatb.2021.120255
Received 9 March 2021; Received in revised form 20 April 2021; Accepted 21 April 2021
Available online 24 April 2021

pure CO_2 instead of syngas, even if the values of CO_2 conversion and CH_3OH selectivity so far achieved do not allow a full commercial exploitation of the catalytic process [23,26]. In this context, to overcome the thermodynamic restrictions typical of methanol synthesis, a viable alternative route to shift the position of CO_2 conversion beyond low conversion values could be represented by the production of DME in presence of a hybrid catalytic system [27,28]. Indeed, equilibrium values of CO_2 conversion and product selectivity, at a typical and stoichiometric feed composition of CO_2/H_2 equal to 1/3 mol/mol, are strongly dependent on temperature and pressure. As a rule, the equilibrium yield of DME increases with pressure and decreases with temperature [29]. What is important is that the CO_2 equilibrium conversion to DME is considerably and consistently higher than that achievable when the conversion is stopped to methanol without further transformation to DME [30], although for maximizing DME selectivity the reaction should be carried out at low temperature. In addition, the thermodynamic limitation of CO_2 conversion could be also mitigated if water is continuously removed from the product side. Several research groups have already confirmed that the direct synthesis of DME using CO_2/H_2 mixture is feasible, but still now the development of a catalyst with suitable properties to operate with both high CO_2 conversion and DME selectivity is a challenge.

The first studies on hybrid/bifunctional catalytic systems active in the direct hydrogenation reaction of CO_2 dealt with the use of physical mixtures between a methanol synthesis catalyst and an acid system, typically a Cu-ZnO-Al_2O_3 system for the synthesis of MeOH and γ-Al_2O_3 or zeolites as acid solids for the dehydration of MeOH. As the name implies, physically mixed hybrid catalysts are prepared by mixing the two catalysts using dry powder mixing or grinding. The characteristic of the physically mixed hybrid catalyst is that both functions, methanol synthesis and methanol dehydration, are preformed before the mixing procedure. Zeolites, in particular, have shown better efficiency than γ-Al_2O_3 as acid components of the bifunctional catalyst, considering that the possibility of modulating acidity (in terms of number, type and strength of acid sites) enables direct synthesis of DME at low temperatures, where the formation of methanol is thermodynamically favored. For instance, Naik et al. [31] compared the catalytic activity of hybrid catalysts prepared by mechanical mixing of a methanol catalyst and γ-Al_2O_3 or ZSM-5 (Si/Al, 60). Catalytic tests carried out in a fixed-bed reactor at 260 °C and 5 MPa revealed that ZSM-5-based bifunctional catalyst exhibits a superior catalytic behaviour than γ-Al_2O_3 supported catalyst, in terms of CO_2 conversion (ca. 30 % vs. ca. 20 %), DME selectivity (ca. 75 % vs. ca. 5%) and stability. As a conclusion, DME yield was about 20 % over methanol catalyst supported on ZSM-5 and lower than 1% over γ-Al_2O_3. Yet, Aguayo et al. [32] investigated the deactivation behavior of Cu−ZnO−Al_2O_3/Na-HZSM-5 and Cu−ZnO−Al_2O_3/γ-Al_2O_3 hybrid catalysts. The bifunctional system was prepared by physical mixing of Cu−ZnO−Al_2O_3 with the methanol dehydration catalyst in an aqueous solution, which was dried subsequently in two steps. Interestingly, the catalyst with Na-HZSM-5 as a solid acid component was less prone to deactivation by coke when water was co-fed, totally recovering its catalytic performance (21 % yield and 48 % selectivity of DME) even after 10 reaction−regeneration cycles. A slight improvement in catalytic activity of Cu−ZnO−Al_2O_3/HZSM-5 was instead observed by addition of Zr as a structural promoter of the bifunctional system [33]. Other types of zeolites in combination with different methanol synthesis catalysts have been evaluated too. Admixtures of Cu−ZnO−ZrO_2 or Cu−ZnO−Ga_2O_3 and NaZSM-5, HZSM-5, H-Ga-silicate or SAPO-34 zeolites were studied extensively by several researchers [34–36]. Combined with Cu−ZnO−ZrO_2, HZSM-5 showed very high DME selectivity (60.1 %) at 35 % CO_2 conversion [35], while H-Ga-silicate showed only 45 % DME selectivity at 19 % CO_2 conversion [34]. In another study, the doping of Zr to Cu−Fe_2O_3/HZSM-5 system was seen to affect the electron density of Cu^{2+}, along with the specific surface area and the reducing behavior of CuO species, definitely enhancing the catalytic activity toward DME [37]. Similarly, Wang et al. [38] examined various Ti/Zr molar ratios in Cu−TiO_2−ZrO_2/HZSM-5, evidencing how the copper reducibility controls the catalytic behaviour. In other studies, addition of small amounts of Pd-decorated carbon nanotubes (CNTs) to a bifunctional Cu−ZrO_2/HZSM-5 system improved the adsorption properties for H_2 and CO_2, in turn increasing the rate of the surface hydrogenation reactions [39]. Also, the catalytic activity could be enhanced using Cu−ZnO−Al_2O_3/HZSM-5 hybrid catalyst supported over acid-treated multi-walled CNTs [40]. Still, Dubois et al. [41] reported a better performance of Y-zeolite (SiO_2/Al_2O_3 = 6), compared to mordenite (SiO_2/Al_2O_3 = 10), in combination with Cu−ZnO−Al_2O_3, as well as a very interesting catalyst performance was exhibited by admixing Cu−ZnO−Cr_2O_3 with NaY, owing to the presence of higher number of moderate acid sites, whereas NaY with only weak acid sites was not effective in DME synthesis [42].

The idea to prepare a multifunctional hybrid system was born by the necessity to overcome the catalytic and technical problems encountered using a mechanical mixture. In particular, considering the limitations of not uniform distribution of active sites, mass transfer constraints, not full reproducibility of the mixed system, …, [43–45], in the last years increasing attention has been paid on novel synthesis strategies to realize a more intimate contact between the methanol synthesis catalyst and the dehydration catalyst. In this respect, several approaches have been reported by different research groups, like the preparation of core–shell hybrid catalysts (with a core of Cu–based catalyst and a shell of a zeolite) [46], the mixing of a zeolite with Cu–ZnO active sites confined in a mesoporous silica [47], the combination of an acid matrix with a Cu-based catalyst supported on carbon nanotubes [48], the immobilization of nanoparticles of CuO and ZnO onto acid supports [49], the mixing of colloidal nanoparticles of Cu/ZnO with γ-Al_2O_3 or HZSM-5 [50,51]. Other studies have shown how the generation both of metal-oxides and acid sites in a single catalyst grain is able to improve the conversion of CO_2 compared to conventional mechanical mixing of a methanol synthesis catalyst and a zeolite, also allowing a higher rate of MeOH formation/dehydration on neighbouring surface sites [52,53]. Nevertheless, there are different opinions on the efficiency of bifunctional catalysts in comparison to admixed systems. García-Trenco et al. [54] stated that the performance of admixed catalyst systems is superior than bifunctional systems, since the classical preparation procedures of bifunctional integrated catalysts lead to a decrease of surface area owing to pores blockage. However, they do not deny that possible interactions among the active components might positively influence catalyst activity. Sun et al. [55] observed an easier generation of DME in presence of a bifunctional catalyst prepared by coprecipitation-sedimentation of a ZrO_2-doped CuZnAl catalyst on a HZSM-5 zeolite, thanks to the close contact among the active sites. Ge et al. [56] also concluded that the active sites need to be in close contact to achieve a synergistic effect for improved catalytic activity, although coverage of active sites during preparation needs to be avoided for possible decrease in active surface area. Qi et al. [57] claimed that addition of Mo to Cu/HZSM-5 (Mo/Cu = 1/2 wt/wt) markedly enhanced the catalytic activity toward DME synthesis by creating new adsorption sites to increase CO_2 hydrogenation rate. Li et al. [58] developed a novel synthesis method to prepare a hybrid catalyst composed of CuO−ZnO as a core and HZSM-5 as a shell layer. The high catalytic activity of core−shell hybrid catalyst was mainly attributed to the orderly self-assembly of core−shell structure, suitable to optimize the reactant diffusion and to enhance the reaction rate. Besides, by inverting the two layers in the core−shell structure, HZSM-5 as shell and Cu−ZnO−Al_2O_3 as a core type capsule catalyst, a good DME selectivity was attained over the conventional hybrid catalyst [58,59].

Frusteri et al. [44] investigated the behaviour of hybrid catalysts prepared via gel-oxalate coprecipitation of CuZnZr precursors in a slurry solution containing ZSM-5 crystals. Results displayed that acidity of zeolite must be carefully tuned as a compromise between catalytic activity and resistance to deactivation by water. Moreover, the microscopy analysis of hybrid systems prepared via co-precipitation of CuZnZr

precursors over zeolites of different topology (*i.e.*, MOR, FER and MFI) revealed that zeolite crystal features strongly affect the metal-oxide(s) distribution, revealing the superior DME productivity of the FER-based catalyst, due to lower mass transfer limitations offered by anchorage of metal-oxide clusters over the lamellar-type crystals as well as a larger population of Lewis basic sites generated on zeolite surface able to activate carbon dioxide and promoting its conversion [60]. Nevertheless, these hybrid integrated catalysts exhibit an important deactivation trend during time-on-stream, mainly favoured by either coke deposition or metal sintering or poisoning from strong water adsorption or contaminants present in the reaction stream, leading to the blockage of active sites [61,62]. In this respect, the addition of Silicalite-1 shell to the ZSM-5 zeolite was considered as an efficient method for improving the resistance to the carbon formation [63]. Very importantly, it has been demonstrated that reactor configuration strongly affects catalyst deactivation, this phenomenon being faster in slurry rather than in fixed-bed reactors [64].

Although hybrid Cu-based systems have been the subject of many research papers reporting catalytic data under a large set of experimental conditions, these examples show that a deeper understanding of the underlying mechanisms and interactions among the active components both in admixed and in bifunctional catalysts is necessary. Therefore, in view of an effective process intensification addressing the scale-up of the catalytic technology, this work has been focused on providing more evidences on the crucial reaction pathways behind the CO_2-to-DME hydrogenation reaction, on the basis of dynamics of surface modifications exhibited during operando investigations by hybrid systems wherein an optimized methanol composition of a CuO–ZnO–ZrO_2 catalyst [43,44] was directly generated on the framework of an acidic ZSM-5 zeolite [65], so to enhance the mutual cooperation among sites of different nature and with a peculiar catalytic role.

2. Experimental

2.1. Synthesis of hybrid CuO–ZnO–ZrO_2/HZSM-5 system

The procedure adopted for the preparation of the CuO–ZnO–ZrO_2/HZSM-5 system consists of a combination of copper, zinc and zirconia with a home-made MFI-type zeolite as described in our previous works [43,44]. The catalyst was synthesized by dissolving copper, zinc and zirconia nitrates in ethanol (Cu/Zn/Zr atomic ratio 6:3:1), following a coprecipitation by oxalic acid at ambient conditions under vigorous stirring in a solution containing a finely dispersed ZSM-5 zeolite (Si/Al, 38 mol/mol; SA, 360 m^2/g; PV, 0.168 cm^3/g; MV, 0.118 cm^3/g). After filtration, drying (95 °C for 16 h) and calcination (350 °C for 4 h), the sample was pelletized at 15 MPa, ground in an agate mortar and sieved for obtaining a size fraction in the range of 40–70 mesh.

2.2. Catalyst characterization

The chemical composition of the samples was determined by ICP-MS (Perkin-Elmer DRC–e), while their morphology along with element distribution was studied by SEM-EDAX analysis (Philips XL-30-FEG).

Regarding the textural properties, nitrogen adsorption/desorption isotherms at −196 °C were performed by using a Micromeritics ASAP 2020 gas adsorption device. The isotherms were elaborated according to the Langmuir method for surface area calculation (*SA*), while Barrett–Joyner–Halenda (BJH) and Horvath-Kawazoe (HK) methods were used for meso- and micro-porosity evaluation.

Measurements of reducibility at temperature programmed (TPR) were performed in a 5 vol.% H_2/Ar mixture, flowing at 30 STP mL/min within a linear quartz micro-reactor (i.d., 4 mm). The experiments were carried out between range 100 and 700 °C at a heating rate of 20 °C/min, monitoring the H_2 consumption by a thermal conductivity detector (TCD), previously calibrated with standard CuO.

Metallic properties were obtained by N_2O chemisorption measurements at 90 °C, assuming a Cu:N_2O = 2:1 titration stoichiometry and a surface atomic density of 1.46×10^{19} Cu_{at}/m^2. Before "single-pulse" N_2O-titration of the metal copper sites, the samples were reduced in situ at 300 °C in flowing H_2 (100 *STP* mL/min) for 1 h, then "flushed" at 310 °C in nitrogen carrier flow (15 min) and further cooled down at 90 °C.

The concentration of acid-base surface sites was determined by temperature programmed desorption of carbon dioxide (CO_2-TPD) and ammonia (NH_3-TPD). The catalysts (ca. 100 mg) were pre-reduced at 300 °C for 1 h under H_2 atmosphere (60 STP mL/min) in a linear quartz micro-reactor (i.d., 4 mm; l, 200 mm). After washing in helium, the samples were saturated for 60 min at 150 °C in an atmosphere of 20 vol.% CO_2/He or 5 vol.% NH_3/He. After baseline stabilization, a carrier flow of He at 25 STP mL/min was used in the temperature range of 100–400 °C or 100–800 °C (heating rate, 10 °C/min) for CO_2 or NH_3 desorption respectively, monitoring their evolution by a thermal-conductivity detector, previously calibrated by pulses of CO_2 or NH_3 at known area.

TEM images of the hybrid catalysts were acquired and elaborated by a Philips CM12 instrument equipped with a high-resolution camera. Powdered samples were dispersed in 2-propanol under ultrasound irradiation and the resulting suspension put drop-wise on a holey carbon-coated support grid.

X-ray photoelectron microscopy (XPS) data were collected on a PHI 5800 spectrometer with a monochromatic Al source. The charging effects were corrected by adjusting the binding energy of C1 s peak from adventitious carbon to 284.6 eV. The characterization experiments were carried out for fresh (before reaction) and spent (after reaction) samples.

2.3. CO_2 hydrogenation by in situ and operando diffuse reflectance FT-IR (DRIFTS) measurements

The nature, functionality and reactivity of surface adsorption sites were probed by *in situ* and *operando* diffuse reflectance FT-IR (DRIFTS) measurements. The spectra under CO_2 hydrogenation conditions (CO_2/H_2, 1:3 mol/mol) were obtained in a Nicolet 5PC Spectrometer equipped with a mid range MCT detector, a KBr beamsplitter, a COLLECTORTM II diffuse reflectance mirror system and a flow-through high temperature DRIFTS cell (Spectra-Tech, Inc.). A ceramic holder cup (i.d.: 5 mm; height: 4 mm) located within a chamber with ZnSe windows was filled up with finely powdered catalyst (14−20 mg) and the experiments were carried out between 200 and 260 °C, at 30 bar, and considering a GHSV of about 60,000 $NL/kg_{cat}/h$. These conditions resulted in very small CO_2 conversions (< 5%), with only formation of methanol, DME and CO, so that the DRIFT cell was considered to be a differential reactor. The resolution was fixed 2 cm^{-1} and the scan speed was adjusted as a function of reaction conditions. Prior to each test, the catalyst was *in situ* reduced at 300 °C for 1 h in pure hydrogen at atmospheric pressure. The reaction at each temperature was stopped only after stabilization of the signals. The evolution of surface species was monitored as a function of reaction temperature either in steady state or in transient mode, wherein one of the reactants (H_2 or CO_2) was selectively removed from the reactant mixture or admitted again inside the reactor cell, until reaching a new steady state, in about 30, 60 or 120 min.

3. Results

3.1. Physico-chemical properties of the hybrid CuO-ZnO-ZrO_2/HZSM-5 catalyst

Differently from the conventional coprecipitation of metal precursors by sodium or potassium carbonate/bicarbonate in aqueous solutions to prepare Cu-based systems, the coprecipitation by oxalic acid in ethanol (gel-oxalate coprecipitation) represents a simple and fast procedure to obtain catalysts free of alkaline contamination, at high level of reproducibility and optimal performance under the typical

conditions of CO_2 hydrogenation [44]. The chemical composition along with the textural properties of the studied sample are reported in Table 1.

It is interesting to observe that no significant change in the chemical composition of the zeolite is visible upon coprecipitation of the methanol synthesis phase, since the atomic Si/Al ratio appears only slightly decreased (36 *vs.* 38) with respect to the bare sample. On the whole, the textural data suggest that copper, zinc and zirconia components distribute over the outer zeolite surface, leading to a hybrid sample characterized by a loss of microporosity (0.026 cm^3/g *vs.* 0.168 cm^3/g of the bare zeolite) and an extended meso-porosity, as evidenced by the increase of the cumulative pore volume (0.374 cm^3/g *vs.* 0.168 cm^3/g of the zeolite).

The multi-site hybridization prompted by the gel-oxalate coprecipitation was probed by TEM and SEM analysis. The TEM image shown in Fig. 1 is illustrative of how the metal-oxide clusters distribute on the zeolite surface. Obviously, the zeolite topology can significantly affect this distribution, with the formation of less or more large agglomerates implying different texture, morphology, surface and also catalytic properties. However, what is important is that the preparation procedure favours a quite uniform distribution of mixed oxides on the zeolite framework, ensuring an intimate surface contact among the phases, predicting minor restrictions in terms of transport phenomena during reaction.

Such a uniform distribution of mixed oxides on the HZSM-5 zeolite is well visible by looking also at the SEM-EDAX micrographs shown in Fig. 2. As displayed, the hybrid catalyst presents a sponge-like structure, typical of porous systems, favouring a long range interdispersion among the different sites onto the zeolite framework.

Fig. 3 shows the XRD pattern of the hybrid CuO-ZnO-ZrO_2/HZSM-5 system upon reduction at 300 °C in H_2 atmosphere. As shown, the characteristic reflections of hexagonal phase of zinc oxide (JCPDS 01−076-0704) and metallic copper (JCPDS 01−089-2838) are well evident, so that the application of the Scherrer's equation to the <111> line of Cu° allowed to determine a mean copper crystallite size of 9.4 nm. Such findings were confirmed by N_2O chemisorptions measurements reported in Table 1 (particle size of ca. 9 nm), accounting for a copper surface area of 27 m^2/g_{cat} and a metal dispersion of 11.1 %.

The reduction behaviour of the hybrid catalyst is shown in Fig. 4. As a reference, the reduction pattern of the pure CuO sample is also reported.

It can be seen that the standard CuO sample exhibits a sharp peak of reduction at 300 °C, diagnostic of a full reduction of CuO to Cu°, while the reduction kinetics of the CuO-ZnO-ZrO_2/HZSM-5 catalyst differs both in terms of pattern and reduction maxima, displaying a main broader peak centered at 257 °C, ascribable to a reactivity of $Cu^{\delta+}$ species strongly affected by a large surface heterogeneity. Moreover, the hydrogen consumption above 350 °C, reporting a convoluted maximum at 600 °C and shouldered on the left side, monitors an incipient reduction of ZnO and/or ZrO_2 in close interaction both with copper crystallites and with the acidic functions of the zeolite [43].

Fig. 5 shows the profiles of CO_2 and NH_3 desorption from the investigated hybrid catalyst. Concerning CO_2-TPD (Fig. 5A), a main convoluted peak shouldered on the high-temperature side points out the contribution of two main sites for CO_2 adsorption, corresponding at weak-medium (below 250 °C) or medium-strong base sites (above 250 °C) respectively.

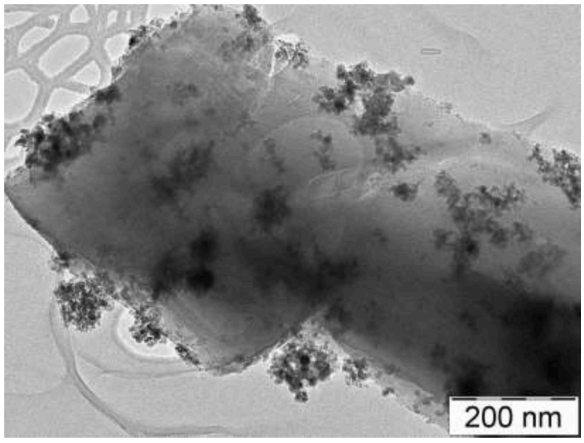

Fig. 1. TEM image of the hybrid CuO-ZnO-ZrO_2/HZSM-5 catalyst.

Specular findings were deduced from NH_3-TPD (Fig. 5B), wherein two main typologies of acid sites were associated both to weak-medium acid sites (100–500 °C), generally inducing a certain proton mobility in zeolites [60], and to medium-strong acid sites (500–800 °C), corresponding to ammonia desorbed from Brønsted acid sites and considered of primary catalytic importance in MeOH-to-DME dehydration reaction [72].

From a quantitative point of view (see Table 2), a cumulative CO_2 capacity of 123 $\mu mol/g_{cat}$ accounts for a prevailing population of weak-medium basic sites (ca. 90 %) mainly concentrated below 250 °C, as diagnostic of surface hydroxyl groups or metal-oxygen pairs [60]. On the other hand, regardless of the typology of acidity (i.e., Brønsted or Lewis), the hybrid catalyst possesses a larger population of weak-medium acid sites (ca. 80 %), evidencing how nature and/or typology of zeolite can significantly affect not only the oxide distribution, but also the surface properties [28,44,60].

XPS analysis was performed in order to obtain information regarding the oxidation state of the elements in the hybrid sample. Their atomic concentration (at.%) (see Table 3) was calculated using HR spectra.

As reported, the sample contains the expected elements (Cu, Zn, Zr, O, Si and C from hydrocarbon contamination). Because of the overlap of the Al 2 s and 2p peaks with the Cu 3 s and 3p peaks and because of the high Cu content, the presence of Al in the zeolite cannot be confirmed. However, the XPS composition clearly deviates from the nominal bulk concentrations, highlighting how the depth distribution of the components is not homogeneous. In particular, the Zr:Cu ratio, which is around 1:2 instead of the nominal 1:6, may be explained by assuming segregation of Zr-oxide clusters to the surface. Moreover, the drastic change of the Cu $L_3M_{45}M_{45}$ Auger line shape upon reduction, along with the

Table 1
Analytical composition, textural and metallic properties of the hybrid CuO-ZnO-ZrO_2/HZSM-5 catalyst.

Cu (at. %)	Zn	Zr	Si/Al[a] (at/at)	SA[b] (m^2/g)	PV[c] (cm^3/g)	MV[d] (cm^3/g)	MSA[e] (m^2/g)	D_{Cu}[f] (%)	d_{Cu}[g] (nm)
58	28	13	36	225	0.374	0.026	27	11.1	9

[a] From ICP measurements.
[b] Surface Area Langmuir.
[c] Pore Volume at p/p0 = 0.995.
[d] Micropore Volume from t-plot.
[e] Copper surface area.
[f] Copper dispersion.
[g] Average Cu particle size.

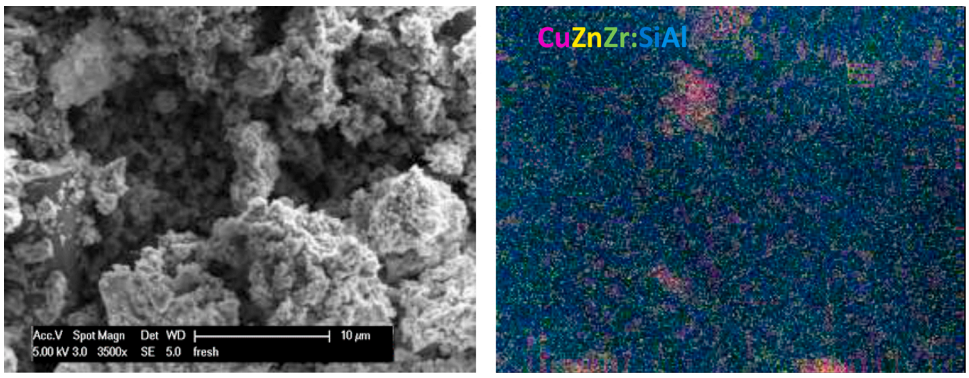

Fig. 2. SEM micrograph and mapping of the "reduced" hybrid CuO-ZnO-ZrO_2/HZSM-5 sample.

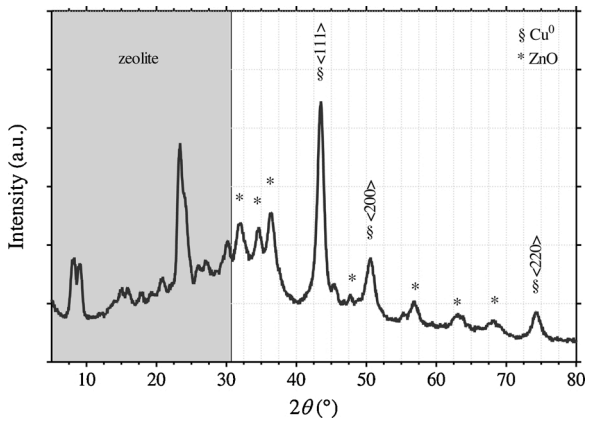

Fig. 3. XRD pattern of the "reduced" hybrid CuO-ZnO-ZrO_2/HZSM-5 sample.

shift of the Cu 2p lines towards lower binding energy and disappearance of some shake-up features (not shown for sake of brevity) indicate the reduction of copper to the metallic state, although a certain fraction of copper resists to be present in oxidized form ($Cu^{\delta+}$). At the same time, the binding energy of 1022.2 eV for Zn $2p_{3/2}$ as well as 182.2 eV for the Zr $3d_{5/2}$ peak are clearly in the range reported for ZnO and ZrO_2 respectively. Finally, the O 1s region (even after correction for the charging of the zeolite-related contribution) presents two main features: the one around 530.3 eV arises from metal-oxides, whereas the other one around 532.2 eV is due to oxygen-containing species in the zeolite. From these observations, it appears that a certain fraction of the oxides is electronically coupled to the zeolite, while another fraction seems to be independent from the zeolite.

3.2. *Dynamics of catalyst surface under relevant CO_2 hydrogenation conditions*

To disclose the nature, functionality and reactivity of the active sites under relevant CO_2 hydrogenation conditions, FTIR-DRIFTS measurements *in operando* mode were performed after contacting the catalyst with a CO_2/H_2 flow (1:3 v/v) at 30 bar for 1 h. In Fig. 6, the spectra acquired at different temperatures (from 200 to 260 °C) were compared and polished from gaseous CO_2, considering the very high intensity of its peaks. No methane, hydrocarbons or coke were detected under the adopted conditions.

The peaks at high wavenumbers (2000−2200 cm^{-1}) are ascribed to gas phase CO, while the ones at 1003-1031−1082 cm^{-1} derive from gas phase methanol [66] and progressively increase with the temperature. Gas phase DME gives relatively sharp bands at 1192, 1176, 1167, 1119, 1100 and 939 cm^{-1}, showing an increase with temperature too. The peak at around 1100 cm^{-1} is generally assigned to methoxy species

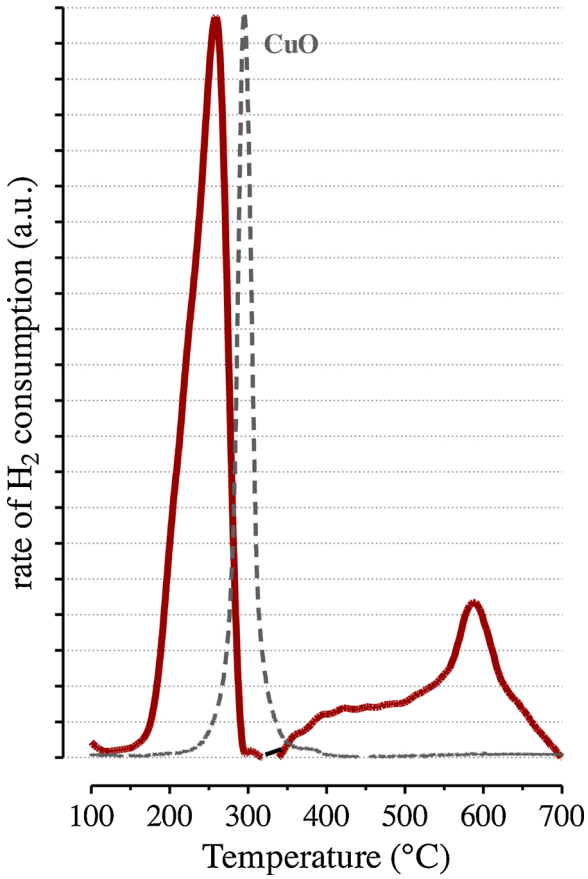

Fig. 4. H_2-TPR profile of the hybrid CuO-ZnO-ZrO_2/HZSM-5 sample. The dashed pattern refers to the reduction of pure CuO.

(CH_3O-) adsorbed on the ZnO component of the catalyst, whereas more complex appears the interpretation of the region 1300−1550 cm^{-1}, considering controversial assignment of C—O stretching either to carbonate/bidentate formate species on Cu [67,68] or to carbonate/hydrogenocarbonate/formate species adsorbed on ZnO [66,69–71].

Moreover, the signal at 1456 cm^{-1} is generally ascribed to the bending of the oxymethylene intermediate on zirconia ($Zr\cdots O_2CH_2$), although this species is reported to be not stable at high temperature [66].

Further DRIFTS experiments were performed in transient mode (see Fig. 7), considering that the behavior of heterogeneous catalyzed reactions is strongly influenced by the rate constant of the elementary steps. Specifically, by exposing the catalyst to changes in partial pressure of the reactants and following the time evolution of the adsorbed species

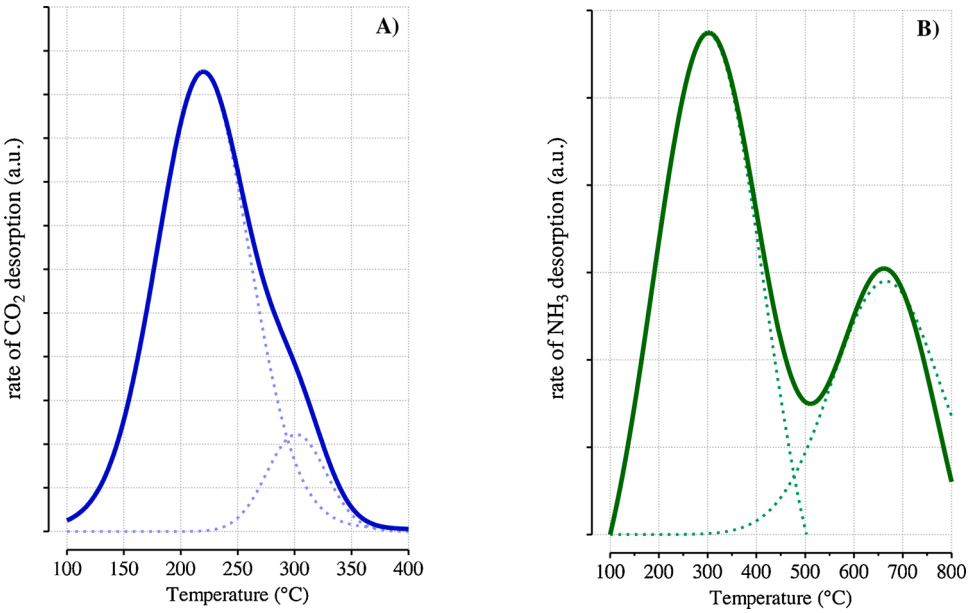

Fig. 5. CO_2-TPD (A) and NH_3-TPD (B) on the hybrid CuO-ZnO-ZrO_2/HZSM-5 catalyst sample.

Table 2
Uptake (μmol/g_{cat}) of CO_2 and NH_3 on the hybrid CuO-ZnO-ZrO_2/HZSM-5 catalyst sample.

CO_2 uptake[(a)]	100–250 °C[(b)]	250–400 °C[(c)]	NH_3 uptake[(d)]	100–500 °C[(e)]	500–800 °C[(f)]
123	109	14	138	112	26

[(a)] Cumulative CO_2 desorption in the range of 100–400 °C.
[(b)] Population of weak-medium base sites between 100 and 250 °C.
[(c)] Population of medium-strong base sites between 250 and 400 °C.
[(d)] Cumulative NH_3 desorption in the range of 100–800 °C.
[(e)] Population of weak-medium acid sites between 100 and 500 °C.
[(f)] Population of medium-strong acid sites between 500 and 800 °C.

Table 3
Composition of the sample as determined from the XPS measurement upon reduction at 300 °C and 300 mbar of H_2 for 1 h.

Element/peak	Binding energy (eV)	Chemical state, relative contribution	at.%
Cu $2p_{3/2}$	932.5	metallic Cu	
Cu LMM Auger parameter	919.1 1851.6	(kinetic energy) metallic Cu CuO	Cu: 5.6
Zn $2p_{3/2}$	1022.2	ZnO	Zn: 4.8
Zr $3d_{5/2}$	182.2	oxidized Zr	Zr: 2.6
O 1 s	530.3 532.2	metal oxides (ZnO, CuO, ZrO_2) SiO_x, -OH	O: 58.4
C 1 s	284.8	Hydrocarbon contamination	C: 9.7
Si 2p	102.2	Si in silicates	Si: 18.9

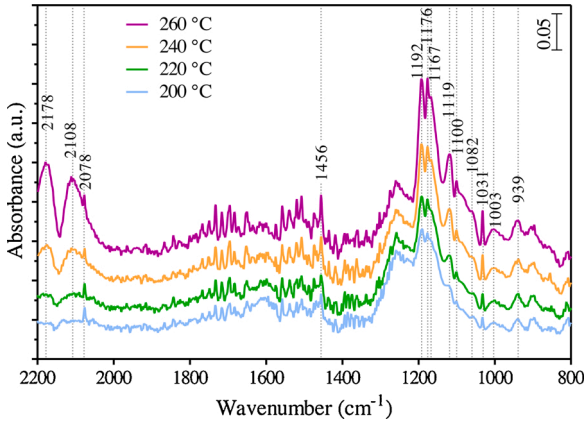

Fig. 6. DRIFTS spectra recorded during the CO_2 hydrogenation reaction from 200 to 260 °C at 30 bar.

under various conditions, it was possible to observe the reactivity of the surface species, with a proper identification of the concomitant spectator surface species. As said, CO_2 and H_2 flows have been alternatively switched off and then re-admitted over the catalyst, thus following the evolution of the adsorbed species with time on stream, as well as the formation of intermediates starting from different initial states.

By analyzing these spectra it is possible to deduce some important information. In fact, after CO_2 switch-off (Fig. 7A), the main peaks related to adsorbed CO, formate, carbonate and methoxy species (at 2075, 1604, 1380, 1303, 1122, 1100, 1082 and 1031 cm^{-1}) decrease in intensity. Instead, the same peaks increase when the flow of CO_2 is admitted onto the catalyst surface again (see Fig. 7B). However, the signal at 1560 cm^{-1} ascribed to bidentate formate (*b*–HCOO-) [71] is still present at the end of the transient step, definitely suggesting that the process of the hydrogenation of *b*–HCOO- represents the rate-limiting step for methanol synthesis from CO_2 hydrogenation. The disappearance of CO during CO_2 switch-off (see Fig. 7A) and its appearance during re-admission of CO_2 (see Fig. 7B) also indicates a direct involvement of carbonate and formate species during reaction, mainly as intermediates to methoxy species. Still, in absence of CO_2 the species adsorbed are fully hydrogenated by H_2 until they disappear (Fig. 7A), whereas they appear

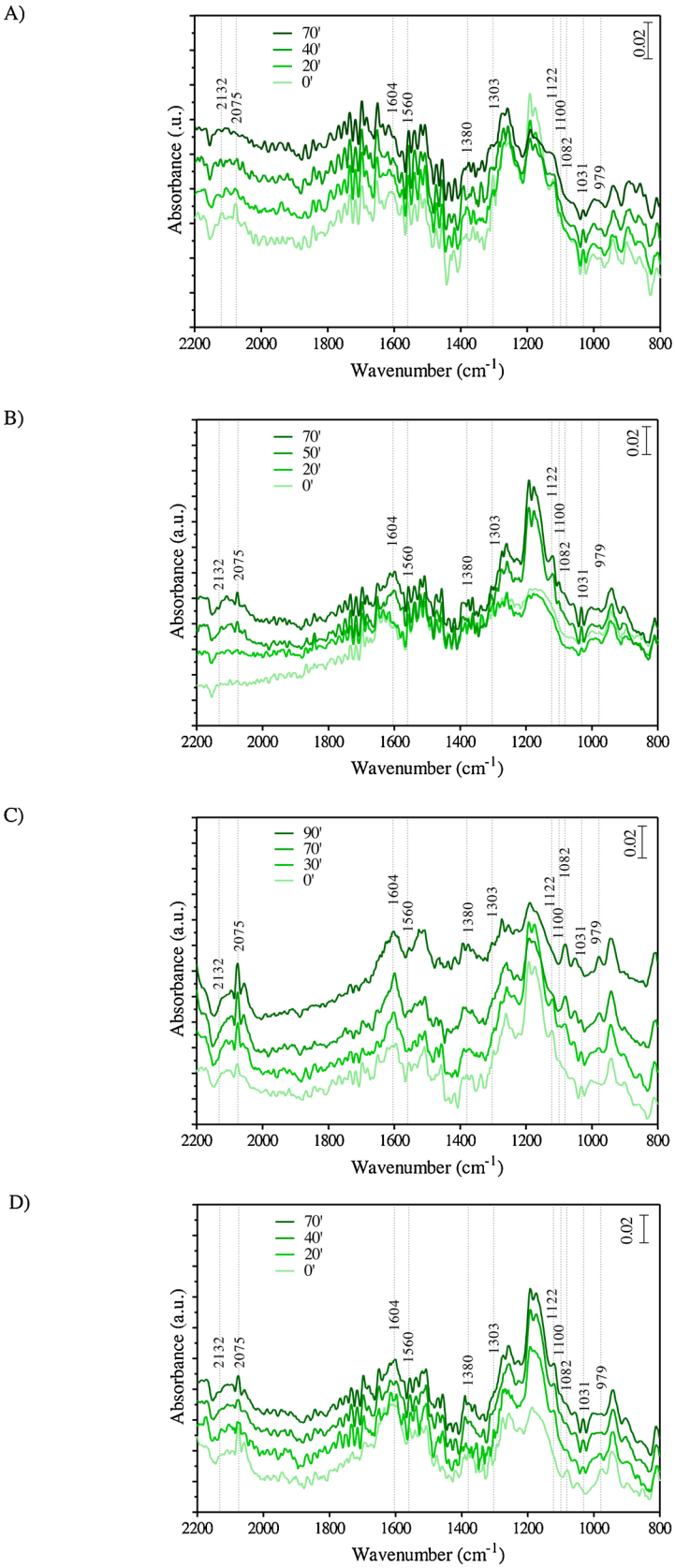

Fig. 7. DRIFTS spectra recorded during the CO_2 hydrogenation reaction at 30 bar and 220 °C in transient mode: A) CO_2 flow switch-off (only H_2 flowing over the catalyst); B) CO_2 flow switch-on; C) H_2 flow switch-off (only CO_2 flowing over the catalyst); D) H_2 flow switch-on.

again when CO_2 pressure is gradually raised and the reaction proceeds with the formation of formate species and production of MeOH and DME (Fig. 7B). Obviously, these modifications require a certain time to take place, more or less long depending on the space velocity.

On the other hand, when H_2 is switched off (see Fig. 7C) the H_2/CO_2 ratio progressively decreases until zeroing, so leading to a progressive disappearance of the signals assigned to the gas phase MeOH and DME signals, contrarily to the signals at 1082 and 979 cm^{-1} assigned to methoxy species adsorbed on ZnO and Cu component respectively, which become more evident. This points out that the hydrogen atom population on the catalyst surface is critically dependent on the H_2/CO_2 ratio and that, in absence of H_2, methoxy species remain adsorbed without undergoing hydrogenation, while the amount of carbonate adsorbed at the metal-oxide interface decreases. Yet, the peak at 1604 cm^{-1}, related to formate (*m*−HCOO-) on metal oxides, decreases consistently with lower H_2 or CO_2 pressure leading to reduced levels of hydrogenation of intermediates and products. As regards the signals in the region 1950−2200 cm^{-1} and specifically the peak at 2075 cm^{-1} derived from CO adsorbed on Cu (111), it decreases during the CO_2 removal (Fig. 7A) consistently with lower carbonate species at 1380 cm^{-1}. It is argued that CO_2 adsorbs dissociatively as CO and surface oxygen (O_s) so that a new CO_2 molecule can form a carbonate species on the surface.

Another important evidence concerns the peak at 2132 cm^{-1} assigned to linear CO adsorbed on $Cu^{\delta+}$ sites which increases during the initial 30', being then removed until to disappear. This unequivocally indicates that the oxidation state of Cu considerably changes during the reaction and that partially oxidized copper particles participate in the catalytic reaction. Finally, in Fig. 7D, by increasing H_2 pressure, the band at 2075 cm^{-1} (assigned to CO adsorbed on Cu) increases with the concentration of CO in gas phase, which proofs a strong competition of H_2 with CO for the adsorption on Cu.

4. Discussion

The main debate about the definition of the real mechanism behind the direct CO_2-to-DME hydrogenation process lays down essentially on the initial step of the whole process, considering the complexity in identifying the activation site of carbon dioxide leading to the formation of methanol as reaction intermediate, then undergoing to dehydration for DME production. In fact, regarding the methanol-to-DME dehydration step most of the studies converge on the existence of two main reaction pathways, according to which either two co-adsorbed methanol molecules associate into DME (associative mechanism) or one molecule of adsorbed methanol is first dissociated into a surface methoxy species then reacting with another methanol molecule to form DME (dissociative mechanism) [72]. Despite specific reaction conditions can significantly address the prevalence of one mechanism on the other one, however for both cases the methanol condensation is consistent with the cooperation of Brønsted acidic sites located on the dehydration component [73–75]. Therefore, the actual debate is more focused on unravelling the mechanistic pathway behind the activation of reactants (i.e., CO_2 and H_2), with a clear definition of the intermediate or spectator species preceding methanol synthesis.

As for CO_2 activation, there are two mechanisms mostly accepted on Cu-based catalysts [76]: (i) formate mechanism, in which CO_2 hydrogenation proceeds via formate intermediates (HCOO); (ii) reverse water-gas shift (RWGS) mechanism, where CO_2 is converted to CO and then to MeOH via hydrogenated intermediates [76–78]. Concerning the formate pathway, kinetic studies have identified the hydrogenation of adsorbed formate (HCOO-) to dioxomethylene (H_2COO-) and adsorbed dioxomethylene to formaldehyde (HCHO-) as the limiting steps for the methanol synthesis [76,78]. The addition of zinc was seen to be effective both in the stabilization of the intermediate HCOOH- by direct Zn-O interaction and in the activation of HCOO- by hydrogenation. On the other hand, the alternative pathway of RWGS has as a limiting step of CO- and formyl (HCO-) hydrogenation. However, it has been demonstrated that on Cu-based surfaces only a small amount of CO- formed via RWGS reaction leads to methanol, most of CO- being more favorably desorbed from the surface, with no effect on methanol selectivity. Therefore, to enhance the catalyst performance, the Cu-based catalysts are typically promoted or doped with various elements, thus improving binding of CO and its hydrogenation to HCO- for facilitating the synthesis of methanol [77,79]. Beside to the parameters affecting product selectivity, like binding energy of adsorbed species and energetics for intermediate reactions, gaseous water produced during reaction is also a critical factor influencing the activation of reactants and triggering possible pathways through carboxyl intermediates [78]. On the whole, an ideal Cu-based catalyst for CO_2 hydrogenation should be able to easily hydrogenate surface intermediates but moderately bond CO, so to favour CO adsorption and progressive hydrogenation without causing any poisoning [75,76].

According to the experimental findings herewith reported, the dissociative H_2 adsorption on the surface of Cu^0 is accompanied by CO_2 adsorption and activation at the metal-oxide interface. Namely, CO_2 dissociatively adsorbs forming CO and surface oxygen with transient formation of carbonate on partially oxidized copper sites (also probed by XPS measurements) [69–71] and then progressive hydrogenation to methoxy via formate, according to the following hydrogenation trend:

O-C-O → (HO−COO-) → HCOO- → HOCHO- → $HOCH_2O$- → CH_2O-(+HO-) → CH_3O-

In particular, as displayed in Fig. 8, the migration of hydrogen atoms by spillover from copper surface to activated CO_2 leads to the formation of either monodentate (*m*−HCOO-) or bidentate formate (*b*−HCOO-). Indeed, hydrogen atoms reach formate species giving rise to the formation of oxo-intermediates preceding methoxy (CH_3O-) formation and finally methanol. Obviously, the feed composition of the hydrogenation stream (i.e., CO or CO_2) significantly affects the Cu oxidation state and accordingly the reaction pathway leading to DME under the same reaction conditions [19,76,78]. Methanol is finally dehydrated to dimethyl ether.

Following the methanol protonation of a methanol molecule on an acidic site of the zeolite, the alcoholic oxygen of the second methanol molecule gives rise to a nucleophilic substitution reaction with the removal of a water molecule and the formation of protonated dimethyl ether. So, a water molecule deprotonates the intermediate transferring back the proton to the zeolite which regenerates the acidic site, and simultaneously, dimethyl ether is formed.

5. Conclusions and future perspectives

Starting from the novel approaches for the development of hybrid catalysts to be employed in the direct hydrogenation of CO_2 to DME, this paper moves a step forward in the definition of the controlling steps of the process and the main intermediates therein involved, also in the light Zof the thermodynamic aspects, suggesting operation at high pressure and low temperature for achieving both high conversion and DME yield. Although Cu−ZnO is expected to remain the benchmark catalyst formulation to activate CO_2, some issues are still associated with the functionality and reactivity of hybrid systems combining a metal-oxide methanol synthesis phase and an acidic methanol dehydration phase to drive the process in one step. In this respect, through a systematic characterization of a CuO-ZnO-ZrO_2/HZSM-5 system, it was demonstrated that metal-oxide(s) components homogeneously distribute over the zeolite surface, ensuring an intimate surface contact among the phases suitable to prevent restrictions in terms of transport phenomena during reaction. In any case, the multi-site nature of the catalyst clearly displays the presence of not unimodal populations of acid or basic sites as well as mutable oxidation states of the copper sites upon activation conditions, affecting the extent of the metal-oxide interface and thus the

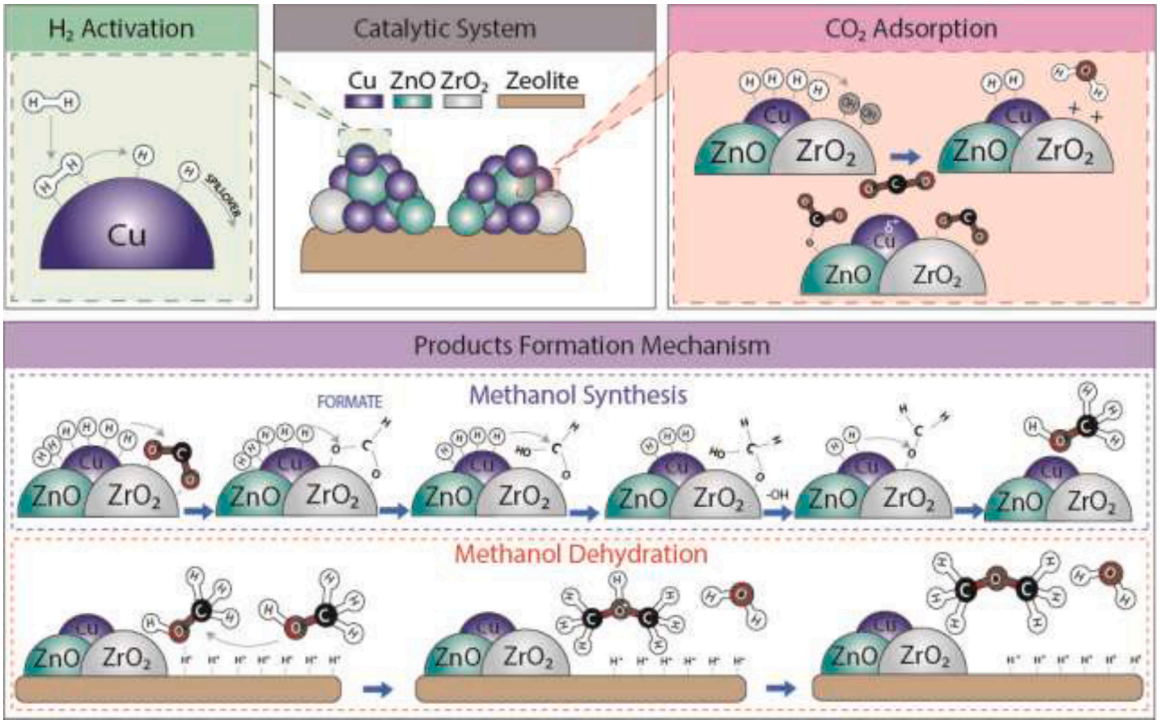

Fig. 8. Proposed reaction mechanisms for direct DME synthesis from CO_2 hydrogenation.

reactivity of $Cu^{\delta+}$ species. These features are evidently determined by the specific preparation procedure adopted, which in the case of the gel-oxalate coprecipitation of metal precursors in a slurry solution of dispersed zeolite leads to the segregation of some cluster oxides to the surface.

Operando spectroscopic investigations under relevant CO_2 hydrogenation conditions allowed to get a deep understanding about the multiple catalytic steps behind DME synthesis, providing crucial information for a rational design of hybrid catalysts. Experiments in steady-state and transient modes confirmed the cooperation of metallic, acid-base and redox sites at a busy gas-solid interface, where the activation of hydrogen atoms, CO and surface oxygen precedes the intermediation of carbonate, formate and methoxy species towards the formation of methanol and then its acid condensation into dimethyl ether.

Looking in a perspective of industrial exploitation, independently of the fact that Cu surfaces or Cu−ZnO interfaces can continue to represent the standard active phase for the catalytic technologies based on CO_2 utilization, nevertheless new synthetic procedures are certainly welcome to realize a better synergy among the phases constituting the hybrid catalyst. Also considering a certain loss of microporosity of the zeolite following the preparation method herewith described, a further research effort is mainly required in tailoring more efficient systems by unconventional procedures, suitable to deliver optimized physico-chemical properties allowing CO_2 activation at a reaction temperature as low as 200 °C, wherein DME selectivity is above 90 %. A challenging target of DME yield close to 30 % can pave the way for a full industrialization of this process, especially if the stability of the system in presence of water as well as the inhibition of other side pathways are fully accomplished.

CRediT authorship contribution statement

Giuseppe Bonura: writing-review & editing, funding acquisition, supervision and project administration. **Serena Todaro:** sample preparation, investigation (XRD, TPR, TPD) and writing-original draft preparation. **Leone Frusteri:** visualization (presentation of data) and writing-original draft preparation. **Izabela Majchrzak-Kucęba:** methodology and supervision from CTU. **Dariusz Wawrzyńczak:** conceptualization and funding acquisition. **Zoltán Pászti:** investigation (XPS measurements and evaluation). **Emília Tálas:** methodology (design of experiments). **András Tompos:** funding acquisition and supervision from TTK. **Lónyi Ferenc:** investigation (evaluation of the operando spectroscopic measurements). **Hanna Solt:** investigation (operando spectroscopic measurements). **Catia Cannilla:** investigation (SEM measurements) and visualization (FTIR-DRIFTS spectra). **Francesco Frusteri:** investigation (TEM measurements and evaluation), writing-review & editing.

Declaration of Competing Interest

The authors report no declarations of interest.

Acknowledgements

This article has been supported by the Polish National Agency for Academic Exchange under Grant No. PPI/APM/2019/1/00042/U/00001.

This project has received funding from the European Union's Horizon 2020 research and innovation programme under grant agreement No. 838061.

The authors acknowledge the bilateral Agreement and the Executive Protocol 2019-2021 between the Hungarian Academy of Sciences (MTA/HAS) and the National Research Council of Italy (CNR) through the project "Inside the reaction mechanism using *in situ* techniques to develop an efficient catalyst for CO_2 conversion into alternative fuels".

References

[1] Z. Azizi, M. Rezaeimanesh, T. Tohidian, M.R. Rahimpour, Chem. Eng. Process. 82 (2014) 150–172, https://doi.org/10.1016/j.cep.2014.06.007.
[2] S.L. Suib, New and Future Developments in Catalysis, Elsevier, Amsterdam, 2013.
[3] E. Peral, M. Martín, Ind. Eng. Chem. Res. 54 (2015) 7465–7475, https://doi.org/10.1021/acs.iecr.5b00823.
[4] R. Steeneveldt, B. Berger, T.A. Torp, Chem. Eng. Res. Des. 84 (2006) 739–763, https://doi.org/10.1205/cherd05049.

[5] T.H. Fleisch, A. Basu, R.A. Sills, J. Nat, Gas Sci. Eng. 9 (2012) 94–107, https://doi.org/10.1016/j.jngse.2012.05.012.
[6] G. Bonura, C. Cannilla, L. Frusteri, A. Mezzapica, F. Frusteri, Catal. Today 281 (2017) 337–344, https://doi.org/10.1016/j.cattod.2016.05.057.
[7] F. Arena, L. Spadaro, O. Di Blasi, G. Bonura, F. Frusteri, Stud. Surf. Sci. Catal. 147 (2004) 385–390, https://doi.org/10.1016/S0167-2991(04)80082-X.
[8] V.M. Lebarbier, R.A. Dagle, L. Kovarik, J.A. Lizarazo-Adarme, D.L. King, D.R. Palo, Catal. Sci. Technol. 2 (2012) 2116–2127, https://doi.org/10.1039/C2CY20315D.
[9] J.W. Jung, Y.J. Lee, S.H. Um, P.J. Yoo, D.H. Lee, K.-W. Jun, J.W. Bae, Appl. Catal. B 126 (2012) 1–8, https://doi.org/10.1016/j.apcatb.2012.06.026.
[10] A. Garcia-Trenco, A. Martinez, Appl. Catal., A 170 (2012) 411–412, https://doi.org/10.1016/j.apcata.2011.10.036.
[11] J.H. Flores, D.P.B. Peixoto, L.G. Appel, R.R. De Avillez, M.I.P.D. Silva, Catal. Today 172 (2011) 218–225, https://doi.org/10.1016/j.cattod.2011.02.063.
[12] S.-C. Baek, S.-H. Kang, J.W. Bae, Y.-J. Lee, D.-H. Lee, K.-Y. Lee, Energy Fuels 25 (6) (2011) 2438–2443, https://doi.org/10.1021/ef200504p.
[13] Y. Luan, Adv. Mat. Res. 183-185 (2011) 183–185, https://doi.org/10.4028/www.scientific.net/AMR.183-185.1505.
[14] J. Palgunadi, I. Yati, K.D. Jung, Reac. Kin., Mech. Catal. 101 (2010) 117–128, https://doi.org/10.1007/s11144-010-0205-z.
[15] P.S.S. Prasad, J.W. Bae, S.H. Kang, Y.J. Lee, K.W. Jun, Fuel Process. Technol. 89 (2008) 1281–1286, https://doi.org/10.1016/j.fuproc.2008.07.014.
[16] K.S. Yoo, J.H. Kim, M.J. Park, S.J. Kim, O.S. Joo, K.D. Jung, Appl. Catal.A. 330 (2007) 57–61, https://doi.org/10.1016/j.apcata.2007.07.007.
[17] F.S. Ramos, A.M. Duarte de Farias, L.E.P. Borges, J.L. Monteiro, M.A. Fraga, E. F. Sousa-Aguiar, L.G. Appel, Catal. Today 101 (2005) 39–44, https://doi.org/10.1016/j.cattod.2004.12.007.
[18] K. Sun, W. Lu, F. Qiu, S. Liu, X. Xu, Appl. Catal., A 252 (2003) 243–249, https://doi.org/10.1016/S0926-860X(03)00466-6.
[19] M. Behrens, F. Studt, I. Kasatkin, S. Kühl, M. Hävecker, F. Abild-Pedersen, S. Zander, F. Girgsdies, P. Kurr, B.-L. Kniep, M. Tovar, R.W. Fischer, J.K. Nørskov, R. Schlögl, Science 336 (2012) 893–897, https://doi.org/10.1126/science.1219831.
[20] M. Poliakoff, W. Leitner, E.S. Streng, Faraday Discuss. 183 (2015), https://doi.org/10.1039/C5FD90078F. 9.
[21] M. Aresta, A. Dibenedetto, E. Quaranta, J. Catal. 343 (2016) 2, https://doi.org/10.1016/j.jcat.2016.04.003.
[22] S. Saeidi, N.A.S. Amin, M.R. Rahimpour, J. CO2 Util. 5 (2014) 66–81, https://doi.org/10.1016/j.jcou.2013.12.005.
[23] G.A. Olah, Angew. Chem. Int. Ed. 52 (2013) 104–107, https://doi.org/10.1002/anie.201204995.
[24] G.A. Olah, A. Goeppert, G.K.S. Prakash, Beyond Oil and Gas:The Methanol Economy, 2nd ed., Wiley-VCH, Weinheim, 2009.
[25] F. Arena, G. Italiano, K. Barbera, S. Bordiga, G. Bonura, L. Spadaro, F. Frusteri, Appl. Catal., A 350 (2008) 16–23, https://doi.org/10.1016/j.apcata.2008.07.028.
[26] J. Ma, N. Sun, X. Zhang, N. Zhao, F. Xiao, W. Wei, Catal. Today 148 (2009) 221–231, https://doi.org/10.1016/j.cattod.2009.08.015.
[27] W.-H. Chen, B.-J. Lin, H.-M. Lee, M.-H. Huang, Appl. Energy 98 (2012) 92–101, https://doi.org/10.1016/j.apenergy.2012.02.082.
[28] G. Bonura, M. Cordaro, C. Cannilla, A. Mezzapica, L. Spadaro, F. Arena, F. Frusteri, Catal. Today 228 (2014) 51–57, https://doi.org/10.1016/j.cattod.2013.11.017.
[29] G. Jia, Y. Tan, Y. Han, Ind. Eng. Chem. Res. 45 (2006) 1152–1159, https://doi.org/10.1021/ie050499b.
[30] W.-J. Shen, K.-W. Jun, H.-S. Choi, K.-W. Lee, Korean J. Chem. Eng. 17 (2000) 210–216, https://doi.org/10.1007/BF02707145.
[31] S.P. Naik, T. Ryu, V. Bui, J.D. Miller, N.B. Drinnan, W. Zmierczak, Chem. Eng. J. 167 (2011) 362–368, https://doi.org/10.1016/j.cej.2010.12.087.
[32] A.T. Aguayo, J. Ereña, I. Sierra, M. Olazar, J. Bilbao, Catal. Today 106 (2005) 265–270, https://doi.org/10.1016/j.cattod.2005.07.144.
[33] Y. Zhao, J. Chen, J. Zhang, J. Nat. Gas Chem. 16 (2007) 389–392, https://doi.org/10.1016/S1003-9953(08)60009-2.
[34] I. Son-Ki, B. Se-Won, P. Young-Kwon, J. Jong-Ki, CO2 Hydrogenation Over Copper-based Hybrid Catalysts for the Synthesis of Oxygenates, Ed. American Chemical Society, Washington, DC, 2003, pp. 183–194.
[35] Q. Ge, Y. Huang, F. Qiu, C. Zhang, J. Nat. Gas Chem. 8 (1999) 28.
[36] G. Bonura, M. Cordaro, L. Spadaro, C. Cannilla, F. Arena, Appl. Catal. B 140−141 (2013) 16–24, https://doi.org/10.1016/j.apcatb.2013.03.048.
[37] R.-w. Liu, Z.-z. Qin, H.-b. Ji, T.-m. Su, Ind. Eng. Chem. Res. 52 (2013) 16648–16655, https://doi.org/10.1021/ie401763g.
[38] S. Wang, D. Mao, X. Guo, G. Wu, G. Lu, Catal. Commun. 10 (2009) 1367–1370, https://doi.org/10.1016/j.catcom.2009.02.001.
[39] M.-H. Zhang, Z.-M. Liu, G.-D. Lin, H.-B. Zhang, Appl. Catal., A 451 (2013) 28–35, https://doi.org/10.1016/j.apcata.2012.10.038.
[40] F. Zha, H. Tian, J. Yan, Y. Chang, Appl. Surf. Sci 285 (Part B) (2013) 945–951, https://doi.org/10.1016/j.apsusc.2013.06.150.
[41] J.L. Dubois, K. Sayama, H. Arakawa, Chem. Lett. 21 (1992) 1115–1118, https://doi.org/10.1246/cl.1992.1115.
[42] K.-W. Jun, K.S. Rama Rao, M.-H. Jung, K.-W. Lee, Bull. Korean Chem. Soc. 19 (1998) 466–470.
[43] F. Frusteri, M. Cordaro, C. Cannilla, G. Bonura, Appl. Catal. B 162 (2015) 57–65, https://doi.org/10.1016/j.apcatb.2014.06.035.
[44] F. Frusteri, G. Bonura, C. Cannilla, G. Drago Ferrante, A. Aloise, E. Catizzone, M. Migliori, G. Giordano, Appl. Catal. B 176 (2015) 522–531, https://doi.org/10.1016/j.apcatb.2015.04.032.
[45] G. Bonura, C. Cannilla, L. Frusteri, F. Frusteri, Appl. Catal., A 544 (2017) 21–29, https://doi.org/10.1016/j.apcata.2017.07.010.
[46] G. Yang, M. Thangkam, T. Vitidsant, Y. Yoneyama, Y. Tan, N. Tsubaki, Catal. Today 171 (2011) 229–235, https://doi.org/10.1016/j.cattod.2011.02.021.
[47] A. García-Trenco, A. Martínez, Appl. Catal., A 493 (2015) 40–49, https://doi.org/10.1016/j.apcata.2015.01.007.
[48] Q. Zhang, Y.-Z. Zuo, M.-H. Han, J.-F. Wang, Y. Jin, F. Wei, Catal. Today 150 (2010) 55–60, https://doi.org/10.1016/j.cattod.2009.05.018.
[49] M. Gentzen, W. Habicht, D.E. Doronkin, J.-D. Grunwaldt, J. Sauer, S. Behrens, Catal. Sci. Technol. 6 (2016) 1054–1063, https://doi.org/10.1039/C5CY01043H.
[50] A. García-Trenco, E.R. White, M.S.P. Shaffer, C.K. Williams, Catal. Sci. Technol. 6 (2016) 4389–4397, https://doi.org/10.1039/C5CY01994J.
[51] A.T. Aguayo, J. Ereña, D. Mier, J.M. Arandes, M. Olazar, J. Bilbao, Ind. Eng. Chem. Res. 46 (2007) 5522–5530, https://doi.org/10.1021/ie070269s.
[52] J. Ereña, J. Vicente, A.T. Aguayo, A.G. Gayubo, M. Olazar, J. Bilbao, Int. J. Hydrogen Energy 38 (2013) 10019–10028, https://doi.org/10.1016/j.ijhydene.2013.05.134.
[53] A. Garcìa-Trenco, S. Valencia, A. Martìnez, Appl. Catal., A 468 (2013) 102–111, https://doi.org/10.1016/j.apcata.2013.08.038.
[54] A. García-Trenco, A. Vidal-Moya, A. Martínez, Catal. Today 179 (2012) 43–51, https://doi.org/10.1016/j.cattod.2011.06.034.
[55] K. Sun, W. Lu, M. Wang, X. Xu, Catal. Commun. 5 (2004) 367–370, https://doi.org/10.1016/j.catcom.2004.03.012.
[56] Q. Ge, Y. Huang, F. Qiu, S. Li, Appl. Catal., A 167 (1998) 23–30, https://doi.org/10.1016/S0926-860X(97)00290-1.
[57] G.-X. Qi, J.-H. Fei, X.-M. Zheng, Z.-Y. Hou, Catal. Lett. 72 (2001) 121–124, https://doi.org/10.1023/A:1009049513834.
[58] Q. Li, C. Xin, P. Lian, Pet. Sci. Technol. 30 (2012) 2187–2195, https://doi.org/10.1080/10916466.2010.512883.
[59] R. Liu, H. Tian, A. Yang, F. Zha, J. Ding, Y. Chang, Appl. Surf. Sci. 345 (2015) 1–9, https://doi.org/10.1016/j.apsusc.2015.03.125.
[60] F. Frusteri, M. Migliori, C. Cannilla, L. Frusteri, E. Catizzone, A. Aloise, G. Giordano, G. Bonura, J. CO2 Util 18 (2017) 353–361, https://doi.org/10.1016/j.jcou.2017.01.030.
[61] D. Jin, B. Zhu, Z. Hou, J. Fei, H. Lou, X. Zheng, Fuel 86 (2007) 2707–2713, https://doi.org/10.1016/j.fuel.2007.03.011.
[62] M. Stiefel, R. Ahmad, U. Arnold, M. Döring, Fuel Process. Technol. 92 (2011) 1466–1474, https://doi.org/10.1016/j.fuproc.2011.03.007.
[63] A. Rownaghi, F. Rezaei, M. Stante, J. Hedlund, Appl. Catal. B 119 (2012) 56–61, https://doi.org/10.1016/j.apcatb.2012.02.017.
[64] F. Raoof, M. Taghizadeh, A. Eliassi, F. Yaripour, Fuel 87 (2008) 2967–2971, https://doi.org/10.1016/j.fuel.2008.03.025.
[65] A. Aloise, A. Marino, F. Dalena, G. Giorgianni, M. Migliori, L. Frusteri, C. Cannilla, G. Bonura, F. Frusteri, G. Giordano, Micropor. Mesopor. Mat. 302 (2020) 110198, https://doi.org/10.1016/j.micromeso.2020.110198.
[66] S. Bailey, G.F. Froment, J.W. Snoeck, K.C. Waugh, Catal. Letters 30 (1994) 99–111, https://doi.org/10.1007/BF00813676.
[67] G.J. Millar, C.H. Rochester, C. Howe, K.C. Waugh, J. Mol. Phys 76 (1991) 833–849, https://doi.org/10.1080/00268979200101721.
[68] S.G. Neophytides, A.J. Marchi, G.F. Froment, Appl. Catal. A 86 (1992) 45–64, https://doi.org/10.1016/0926-860X(92)80041-A.
[69] J. Saussey, J.C. Lavalley, C. Bovet, J. Chem. Soc. Faraday Trans. I 78 (1982) 1457–1463, https://doi.org/10.1039/F19827801457.
[70] B.A. Sexton, A.E. Hughes, N.R. Avery, Appl. Surf. Sci. 22 (1985) 404–414, https://doi.org/10.1016/0378-5963(85)90072-8.
[71] Q. Sun, C.W. Liu, W. Pan, Q.M. Zhu, J. Fa Deng, Appl. Catal., A 171 (1998) 301–308, https://doi.org/10.1016/S0926-860X(98)00096-9.
[72] E. Catizzone, C. Freda, G. Braccio, F. Frusteri, G. Bonura, J. Energy Chem. 58 (2021) 55, https://doi.org/10.3390/ijerph18020807.
[73] X. Jiang, X. Nie, X. Guo, C. Song, J.G. Chen, Chem. Rev. 120 (2020) 7984–8034, https://doi.org/10.1021/acs.chemrev.9b00723.
[74] A. Aloise, A. Marino, F. Dalena, G. Giorgianni, M. Migliori, L. Frusteri, C. Cannilla, G. Bonura, F. Frusteri, G. Giordano, Microp. Mesop. Mat. 302 (2020) 110198–110205, https://doi.org/10.1016/j.micromeso.2020.110198.
[75] L. Frusteri, G. Bonura, C. Cannilla, S. Todaro, G. Giordano, M. Migliori, F. Frusteri, Petrol. Chem. 60 (2020) 508–515, https://doi.org/10.1134/S0965544120040076.
[76] R. Guil-López, N. Mota, J. Llorente, E. Millán, B. Pawelec, J.L.G. Fierro, R. M. Navarro, Materials 12 (2019) 3902–3925, https://doi.org/10.3390/ma12233902.
[77] I. Ud Din, M.S. Shaharun, M.A. Alotaibi, A.I. Alharthi, A. Naeem, J. CO2 Util 34 (2019) 20–33, https://doi.org/10.1016/j.jcou.2019.05.036.
[78] J. Toyir, P. Ramirez de la Piscina, J.L.G. Fierro, N. Homs, Appl. Catal. B 34 (2001) 255–266, https://doi.org/10.1016/S0926-3373(01)00203-X.
[79] L.C. Grabow, M. Mavrikakis, ACS Catal. 1 (2011) 365–384, https://doi.org/10.1021/cs200055d.